

# Thermal stress implications in athermal TiO<sub>2</sub> waveguides on a silicon substrate

Jock Bovington,\* Rui Wu, Kwang-Ting Cheng, and John E. Bowers

<sup>1</sup>Department of Electrical & Computer Engineering, University of California Santa Barbara, California, USA  
jock@ece.ucsb.edu

**Abstract:** Ring resonators with TiO<sub>2</sub> core confinement factors from 0.07 to 0.42 are fabricated and measured for thermal sensitivity achieving  $-2.9$  pm/K thermal drift in the best case. Materials used are CMOS compatible (TiO<sub>2</sub>, SiO<sub>2</sub> and Si<sub>3</sub>N<sub>4</sub>) on a Si substrate. The under discussed role of stress in thermo-optic behavior is clearly observed when contrasting waveguides buried in SiO<sub>2</sub> to those with etched sidewalls revealed to air. Multiphysics simulations are conducted to provide a theoretical explanation of this phenomenon in contrast to the more widely reported theories on thermo-optic behavior dominated by confinement factor.

©2014 Optical Society of America

**OCIS codes:** (160.3130) Integrated optics materials; (230.7380) Waveguides, channeled; (160.6840) Thermo-optical materials; (130.3120) Integrated optics devices

---

## References and links

1. T. H. Kim, B. G. You, H. J. Lee, and T. H. Rhee, "Athermal AWG multiplexer/demultiplexer for E/C-band WDM-PON application," in *2007 Asia Opt. Fiber Commun. Optoelectron. Conf. 2* (IEEE, 2007), pp. 330–332.
2. N. Ooba, Y. Hibino, Y. Inoue, and A. Sugita, "Athermal silica-based arrayed-waveguide grating multiplexer using bimetal plate temperature compensator," *Electron. Lett.* **36**(21), 1800–1801 (2000).
3. Y. Hibino, M. Abe, T. Tanaka, A. Himeno, J. Albert, D. C. Johnson, and K. O. Hill, "Temperature-insensitive UV-induced Bragg gratings in silica-based planar lightwave circuits on Si," *Electron. Lett.* **35**(21), 1844–1845 (1999).
4. H. Huang, S.-T. Ho, D. Huang, Y. Tu, and W. Liu, "Design of temperature-independent arrayed waveguide gratings based on the combination of multiple types of waveguide," *Appl. Opt.* **49**(16), 3025–3034 (2010).
5. H. Tanobe, Y. Kondo, Y. Kadota, K. Okamoto, and Y. Yoshikuni, "Temperature insensitive arrayed waveguide gratings on InP substrates," *IEEE Photonics Technol. Lett.* **10**(2), 235–237 (1998).
6. M. Uenuma and T. Mooka, "Temperature-independent silicon waveguide optical filter," *Opt. Lett.* **34**(5), 599–601 (2009).
7. V. Raghunathan, W. N. Ye, J. Hu, T. Izuhara, J. Michel, and L. Kimerling, "Athermal operation of silicon waveguides: spectral, second order and footprint dependencies," *Opt. Express* **18**(17), 17631–17639 (2010).
8. P. Alipour, A. Atabaki, A. Eftekhar, and A. Adibi, "Athermal performance in titania-clad microring Resonators on SOI," in *Integrated Photonics Research, Silicon and Nanophotonics and Photonics in Switching*, OSA Technical Digest (CD) (Optical Society of America, 2010), paper IMC6.
9. F. Qiu, A. M. Spring, F. Yu, and S. Yokoyama, "Complementary metal–oxide–semiconductor compatible athermal silicon nitride/titanium dioxide hybrid micro-ring resonators," *Appl. Phys. Lett.* **102**(5), 051106 (2013).
10. S. S. Djordjevic, K. Shang, B. Guan, S. T. S. Cheung, L. Liao, J. Basak, H.-F. Liu, and S. J. B. Yoo, "CMOS-compatible, athermal silicon ring modulators clad with titanium dioxide," *Opt. Express* **21**(12), 13958–13968 (2013).
11. B. Guha, J. Cardenas, and M. Lipson, "Athermal silicon microring resonators with titanium oxide cladding," *Opt. Express* **21**(22), 26557–26563 (2013).
12. T. D. Visser, H. Blok, B. Demeulenaere, and D. Lenstra, "Confinement factors and gain in optical amplifiers," *IEEE J. Quantum Electron.* **33**(10), 1763–1766 (1997).
13. M. Huang and X. Yan, "Thermal-stress effects on the temperature sensitivity of optical waveguides," *J. Opt. Soc. Am. B* **20**(6), 1326–1333 (2003).
14. A. Arbabi and L. L. Goddard, "Measurements of the refractive indices and thermo-optic coefficients of Si<sub>3</sub>N<sub>4</sub> and SiO<sub>x</sub> using microring resonances," *Opt. Lett.* **38**(19), 3878–3881 (2013).
15. C. Ottermann and K. Bange, "Correlation between the density of TiO<sub>2</sub> films and their properties," *Thin Solid Films* **286**(1–2), 32–34 (1996).
16. M. Huang, "Stress effects on the performance of optical waveguides," *Int. J. Solids Struct.* **40**(7), 1615–1632 (2003).
17. C. Ottermann, R. Kuschneireit, O. Anderson, P. Hess, and K. Bange, "Young's modulus and density of thin TiO<sub>2</sub> films produced by different methods," *Mater. Res. Soc.* **436**, 251–256 (1996).
18. "Stress-optical effects with generalized plane strain." COMSOL Multiphysics 4.3a (2012).

19. A. Khan, J. Philip, and P. Hess, "Young's modulus of silicon nitride used in scanning force microscope cantilevers," *J. Appl. Phys.* **95**(4), 1667–1672 (2004).
20. National Physical Laboratory Kaye and Laby Table of Physical and Chemical Constants, Version 1.1,(2010), [http://www.kayelaby.npl.co.uk/general\\_physics/2\\_3/2\\_3\\_5.html](http://www.kayelaby.npl.co.uk/general_physics/2_3/2_3_5.html). Accessed Sept. 4, 2013.
21. C.-C. Lee, C.-L. Tien, W.-S. Sheu, and C.-C. Jaing, "An apparatus for the measurement of internal stress and thermal expansion coefficient of metal oxide films," *Rev. Sci. Instrum.* **72**(4), 2128–2133 (2001).
22. P. Temple-Boyer, C. Rossi, and E. Scheid, "Residual stress in low pressure chemical vapor deposition SiNx films deposited from silane and ammonia," *J. Vac. Sci. Technol. A* **16**(4), 2003–2007 (1998).

---

## 1. Introduction

Thermal stability is an important topic in integrated photonics research. The need for athermal structures is clear for photonics applications from low-cost communications links in data centers, passive optical networks, microwave photonic filters, and sensors. The current solutions use single channels, coarse wavelength division multiplexing (CWDM), temperature stabilizing feedback loops, or a power hungry thermo-electric cooler (TEC).

This is an active research area with a number of solutions to address the thermal stability challenge by designing intrinsically athermal structures. We would classify them into packaging solutions [1–3], circuit based approaches [4–6], and materials solutions. Among the materials solutions, the overwhelming majority have used polymers [7]. Oft-quoted issues with these polymer-based solutions include process compatibility, performance degradation, long-term reliability, and narrowed operating temperature conditions. Much work to address these concerns continues, and in the end such solutions may become practical. However, titania (TiO<sub>2</sub>) has been suggested as a CMOS compatible alternative material to polymers for enabling athermal waveguides in photonic integrated circuits [8]. The reason for this is its strong negative material thermo-optic coefficient (TOC)  $dn/dT$ . Literature has quoted its TOC in a range of  $-(1-6.5) \times 10^{-4} \text{ K}^{-1}$  partially due to its deposition method [8–10]. However, we postulate different stress profiles as one cause for this wide variation.

In this paper we present some experiments with ring resonators offering a clean and repeating spectral signature that one can track even with only small deviations in their resonance wavelengths. A resonator is also an important device for the proposed WDM systems and would therefore greatly benefit from thermal stabilization for uncooled systems. The rings presented use TiO<sub>2</sub> as a core material rather than a cladding layer, as previously demonstrated [9,10].

Our measurements indicate that buried TiO<sub>2</sub> core waveguides clad by plasma enhanced chemical vapor deposition (PECVD) SiO<sub>2</sub> with core confinements ranging from 0.07 to 0.42 exhibit  $dn_{\text{eff}}/dT$  on the order of the published SiO<sub>2</sub> TOC ( $\sim 10^{-5} \text{ K}^{-1}$ ) regardless of confinement. This implies a TOC of TiO<sub>2</sub> at  $\sim 10^{-6} \text{ K}^{-1}$ , two orders of magnitude less than the literature values. We argue that in such geometries the thermo-stress-optic (TSO) effect can dominate the TOC, which contradicts current literature on athermal waveguides which use a confinement factor model without dispersion, thermal path length expansion, and stress considerations [8–11]. Given the results discussed in Section 3, we developed theory and conducted simulations to explain our experimental results.

## 2. Waveguide geometry and fabrication

A single lithography process with a chromium hard mask was used for all waveguides. 15μm of thermal oxide was grown to eliminate potential substrate leakage for thin core geometries. Amorphous TiO<sub>2</sub> was DC sputtered at 2300W in an Ar/O<sub>2</sub> (20/10sccm) environment with a Ti target at room temperature in an Endeavor tool. The measured index was 2.18 at 1550nm as measured in a J.A. Woollam Co. Inc variable angle spectroscopic ellipsometer (VASE). Si<sub>3</sub>N<sub>4</sub> was deposited using low pressure chemical vapor deposition on both sides of the wafer using a stoichiometric process with a refractive index of 1.98 at 1550nm as measured in the VASE. High density PECVD SiO<sub>2</sub> films used as cladding above the core were deposited at 300°C. Lithography was done using an ASML PAS 5500/300 deep ultra-violet photolithography tool. Dry etching was done with an inductively coupled plasma etcher for the Cr hardmask with a

Cl<sub>2</sub>/O<sub>2</sub> chemistry, followed by a CHF<sub>3</sub>/CF<sub>4</sub>/O<sub>2</sub> dry-etch of the core. This core etch sufficiently removed the photo-resist softmask such that only the Cr remained. The Cr was then dry-etched. The revealed core was cleaned with O<sub>2</sub> plasma to remove the remaining polymer from the ICP etches. Buried waveguides had additional PECVD SiO<sub>2</sub> over cladding. The samples were then diced and tested as described below in Section 3. Figure 1 below shows the three waveguide cross sections reported in this work.

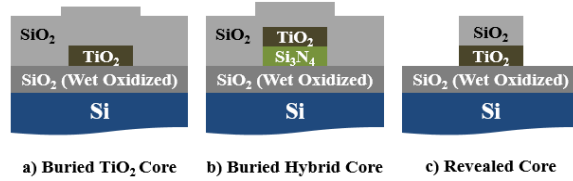


Fig. 1. Cross section of waveguide designs with TiO<sub>2</sub> or hybrid cores.

### 3. Measurement setup and results

Using a tunable laser, polarization controller, lensed fiber facet coupling and a photodiode, we tracked the TE resonance of the through port of ring resonators with temperature (15-40°C) for a range of waveguide geometries (widths, thicknesses and radii) with 0.07 to 0.42 material confinement factors simulated in Fimmwave. This diverse set was used to span a large range of confinement factors. These measurements are plotted in Fig. 2(a) with simulations using a confinement model detailed in Section 4. Geometry details are provided in Table 1. Figure 2(b) adds measurements from two sources which reported a range of geometries [10,11]. Our buried structures clearly stand out in these data sets as having negligible change in thermal drift with increasing TiO<sub>2</sub> confinement. From this we conclude that the TiO<sub>2</sub> TOC is effectively suppressed to  $\sim 10^{-6} \text{K}^{-1}$  by burying these TiO<sub>2</sub> cores. This effect is released when the sidewall of the TiO<sub>2</sub> is revealed by co-etching the top cladding and the core as shown in Fig. 1(c). These revealed structures fit a confinement factor model described in Section 4 with a TOC of  $-2.5 \times 10^{-4} \text{K}^{-1}$  which is more comparable to the UC Davis and Cornell results using TiO<sub>2</sub> as a top cladding which also lacks a thermal stress of top SiO<sub>2</sub> cladding.

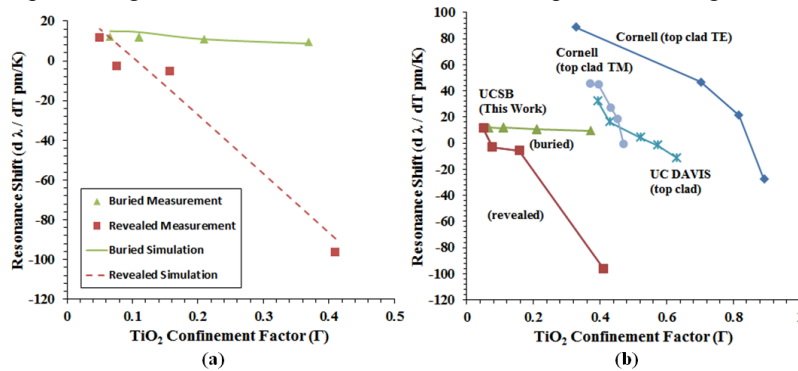


Fig. 2. (a) Measured thermal drift with separate confinement models simulated for buried and revealed rings. (b) Measurements compared to other literature with TiO<sub>2</sub> cladding demonstrates a suppression of TOC in buried TiO<sub>2</sub>.

### 4. Theory and simulation

The analysis in Section 3 results in two separate TOCs for the same TiO<sub>2</sub> material processed in nearly identical conditions, which is in contrast to an intuitive understanding of TOC as a geometrically independent parameter. Therefore, further exploration was conducted to converge on a model which explains these measurements.

The most typical model we have found for thermal drift is a *confinement model*. Below is a derivation of this model for a ring resonator with resonance wavelength  $\lambda_r$ .

$$m\lambda_r = 2\pi n_{\text{eff}}(\lambda_r, T)R(T)$$

$$\frac{d\lambda_r}{dT} = \frac{n_{\text{eff}}\lambda_r}{n_g R} \frac{\partial R}{\partial T} + \frac{\lambda_r}{n_g} \frac{\partial n_{\text{eff}}}{\partial T} \approx \frac{\lambda_r}{n_g} \left( n_{\text{eff}}\alpha_{\text{sub}} + \frac{\partial n_{\text{eff}}}{\partial T} \right) \quad (1)$$

$$\text{where, } \frac{\partial n_{\text{eff}}}{\partial T} \approx \sum_k \Gamma_k \frac{\partial n_k}{\partial T}. \quad (2)$$

The ring radius,  $R$ , and the effective index,  $n_{\text{eff}}$ , are explicitly a function of temperature,  $T$ , and  $m$  is the longitudinal mode number. The ring radius is cancelled out and not in the final Eq. (1). The use of partial derivative in  $\partial n_k / \partial T$  implies the term is only a function of temperature. The material confinement factor,  $\Gamma$  as define by Visser et al. in [12], quantifies the overlap of the optical mode with each material  $k$ . The resulting  $\partial n_{\text{eff}} / \partial T$  is the sum over all  $k$  materials in which the light interacts. The final assumption is that the expansion of the actual waveguide path length is dominated by the linear thermal expansion of the 525 $\mu\text{m}$  Si substrate  $\alpha_{\text{sub}}$ .

Below is an alternative derivation for a *combined model* including stress terms similar to [2,13]. Throughout this derivation a short hand has been used for the stress tensor  $\sigma$ .

$$m\lambda_r = 2\pi n_{\text{eff}}(\lambda_r, \sigma, T)R(\sigma, T)$$

$$\frac{d\lambda_r}{dT} = \frac{\lambda_r}{n_g} \left( \frac{\partial n_{\text{eff}}}{\partial \sigma} \frac{d\sigma}{dT} + \frac{\partial n_{\text{eff}}}{\partial T} \right) + \frac{n_{\text{eff}}\lambda_r}{n_g R} \frac{\partial R}{\partial \sigma} \frac{d\sigma}{dT} + \frac{n_{\text{eff}}\lambda_r}{n_g R} \frac{\partial R}{\partial T} \quad (3)$$

$$\frac{d\lambda_r}{dT} \approx \frac{\lambda_r}{n_g} \left( n_{\text{eff}}\alpha_{\text{sub}} + \frac{dn_{\text{eff}}}{dT} + \beta \frac{d\sigma}{dT} \right)$$

$$\text{where, } \frac{dn_{\text{eff}}}{dT} \equiv \frac{\partial n_{\text{eff}}}{\partial \sigma} \frac{d\sigma}{dT} + \frac{\partial n_{\text{eff}}}{\partial T}. \quad (4)$$

In addition to the confinement term  $\partial n_{\text{eff}} / \partial T$  used in Eq. (1), a stress term is added to the  $dn_{\text{eff}} / dT$ . This term incorporates the stress dependent TOC. All dispersion effects are accounted for in the group index  $n_g$ . There is also a stress induced path length change term with a device dependent constant tensor  $\beta$ , which is significant when packaging a device such as in [1–3]. For the purposes of devices in Table 1, this term is assumed to be negligible in comparison to the  $\alpha_{\text{sub}}$  as the symmetric thermal oxide prevents bowing and no packaging is used to induce further thermal stress.

Three models are presented in Table 1 and plotted in Fig. 3, the *confinement model*, the *stress model*, and the *combined model*. The *stress model* is the same as the *combined model*,

**Table 1. Comparison of thermo-optic models and measured data**

	Ring Geometries				Confinement					$d\lambda_r / dT$ (pm/K)			
	$w$ ( $\mu\text{m}$ )	$t_{\text{TiO}_2}$ (nm)	$t_{\text{Si}_3\text{N}_4}$ (nm)	$R$ ( $\mu\text{m}$ )	$\text{TiO}_2$	$\text{SiO}_2$	$\text{Si}_3\text{N}_4$	$n_g$	$n_{\text{eff}}$	Meas.	Conf. Model	Stress Model	Comb. Model
Buried	4	30	90	1232	0.07	0.78	0.18	1.66	1.51	11.8	7.0	3.1	30.4
	4	45.6	90	1232	0.11	0.73	0.20	1.72	1.53	11.5	1.7	3.2	22.3
	4	90	0	1232	0.21	0.82	0	1.67	1.51	10.8	-14.2	3.2	2.3
	4	135	0	1232	0.37	0.67	0	1.84	1.58	9.48	-31.6	5.01	-4.2
	0.9	180	0	40	0.41	0.49	0	2.00	1.50	-96.3	-34.6	-39.7	-61.4
Revealed	4	75	0	1232	0.16	0.87	0	1.62	1.48	-5.60	-14.8	-12.8	-32.9
	4	50	0	1232	0.08	0.94	0	1.54	1.46	-2.93	3.1	-11.4	-5.2
	20	40	0	1530	0.05	0.96	0	1.51	1.46	11.7	6.9	-4.5	1.8
											$B_1 (10^{-12}/\text{Pa}) =$	0	-1000
										$B_2 (10^{-12}/\text{Pa}) =$	0	1000	0.5
										$dn_{\text{TiO}_2} (\times 10^{-5}) / dT =$	-13	0	-18

however it assumes that  $\partial n_{eff}/\partial T = 0$ . To calculate the three models in Table 1 below we use COMSOL finite element stress-optic simulations in 2 dimensions with a generalized plane strain model to solve for Eq. (4) and Fimmwave film mode matching model for accurate confinement factors, effective indices, and group indices for the fundamental TE mode. Unless otherwise stated, we used the material properties in Table 2.

Values for  $B_1$  and  $B_2$  are not reported in the literature for sputtered  $TiO_2$  or LPCVD  $Si_3N_4$  so it is not possible to validate them without additional measurements. These should be pursued for precise values for these parameters.

**Table 2. Material Properties for Simulation ( $\lambda_0 = 1550nm$ )**

	$TiO_2$	$SiO_2$	$Si_3N_4$	$Si$
n	2.18 <sup>b</sup>	1.445 <sup>b</sup>	1.98 <sup>b</sup>	3.478
$dn(\times 10^{-5})/dT$	-(10-65) <sup>a</sup>	1	2.4 [14]	18 [8]
$B_1 (10^{-12}/Pa)$	<sup>a</sup>	0.65 [15]	~0.65 <sup>d</sup>	-11.35 [16] <sup>c</sup>
$B_2 (10^{-12}/Pa)$	<sup>a</sup>	4.2 [15]	~4.2 <sup>d</sup>	3.65 [16] <sup>c</sup>
$\nu$	0.2 [17]	0.42 [18]	0.2 [19]	0.19 [18]
$E (GPa)$	65 [17]	78 [18]	285 [19]	110 [18]
$\rho (g/cm^3)$	3 [15]	2.203 [18]	3.1 [19]	2.33 [18]
$\alpha(10^{-6}/K)$	7.5 [20]	0.38 [21]	3.0 [22]	2.6 [20]

<sup>a</sup>Least squares fit, <sup>b</sup>Measured, <sup>c</sup>Anisotropic tensor is more accurate, <sup>d</sup>Assumed for lack of literature

Young's modulus  $E$ , Poisson's ratio  $\nu$ , and linear thermal expansion coefficients  $\alpha$  for all materials including the silicon substrate are shown in Table 2. Refractive indices relate with the thermal stress as described by three stress-optic coefficients  $B_1$  and  $B_2$ , and  $B_3$ . In the case of an isotropic material, as we have assumed  $SiO_2$ ,  $Si_3N_4$ , and  $TiO_2$  to be,  $B_3 = B_1 - B_2$ . In Eq. (5)  $n_0$  is the scalar index without stress, and  $dn_{ij}$  and  $\sigma_{ij}$  are the stress induced index change and stress coefficients of  $\sigma$  respectively. As  $n_{ij}$  and  $\sigma_{ij}$  are functions of temperature,  $T$ , and we are interested in their derivatives, the cross terms which relate to  $B_3$  are not negligible, however  $\sigma_{xz}$  and  $\sigma_{yz}$  reduce to zero under the assumptions of the generalized plane strain model.

$$\begin{bmatrix} dn_{xx} \\ dn_{yy} \\ dn_{zz} \\ dn_{yz} \\ dn_{xz} \\ dn_{xy} \end{bmatrix} = \begin{bmatrix} n_{xx} - n_0 \\ n_{yy} - n_0 \\ n_{zz} - n_0 \\ n_{yz} - 0 \\ n_{xz} - 0 \\ n_{xy} - 0 \end{bmatrix} = \begin{bmatrix} B_1 & B_2 & B_2 & 0 & 0 & 0 \\ B_2 & B_1 & B_2 & 0 & 0 & 0 \\ B_2 & B_2 & B_1 & 0 & 0 & 0 \\ 0 & 0 & 0 & B_3 & 0 & 0 \\ 0 & 0 & 0 & 0 & B_3 & 0 \\ 0 & 0 & 0 & 0 & 0 & B_3 \end{bmatrix} \begin{bmatrix} \sigma_{xx} \\ \sigma_{yy} \\ \sigma_{zz} \\ \sigma_{yz} \\ \sigma_{xz} \\ \sigma_{xy} \end{bmatrix} \quad (5)$$

In addition to Table 1  $d\lambda_r/dT$  all three models are plotted against the measurements in Fig. 3. It is clear from this figure the difference in the models. The *confinement model* in Fig. 3(a) doesn't result in a different thermal drift behavior between buried and revealed waveguides as seen in measurements. The *stress model* in Fig. 3(b), fitting for  $B_1$  and  $B_2$ , shows a split between the two waveguide types and fits the data better than the *confinement model* when compared using an F test ( $\alpha = 0.1$ ) to rule out the addition of a fit parameter. However, the values  $B_1$  and  $B_2$  derived from the *stress model* fit are probably non-physical as they are quite large. In contrast the *combined model* which fits for  $B_1$ ,  $B_2$ , and the TOC of  $TiO_2$  has a better least squares fit, but doesn't quite pass the F test ( $\alpha = 0.1$ ) as the superior model given it uses 3 fit parameters. However, this is backed by a clear physical model and has parameters which are reasonable. This comparison may also be confounded by the large variation in waveguide geometries which was required to span such a larger range of low confinements. By far and away the best model was a separate confinement model for each

type of waveguide as shown in Fig. 2(a). Given most analyses will only use waveguides of a similar stress profile and geometry, this may be a practical model, however we do emphasize that it lumps all of the underlying physics into a single non-generalizable parameter which cannot be fairly compared between a diverse set of literature as is apparent in the range of TiO<sub>2</sub> TOCs already reported.

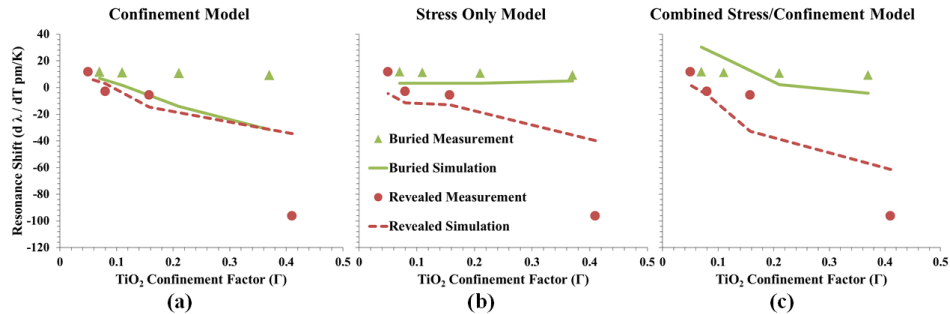


Fig. 3. Comparison of the (a) confinement, (b) stress, and (c) combined stress/confinement models.

Figure 4 plots the thermally induced stress profiles of characteristic revealed and buried waveguides showing the contrast of those stresses applied to the core and adjacent cladding. As is clear from the plots, these waveguides have complex and drastically different thermal stress profiles; which may cause the large difference in thermal drift uncorrelated to TiO<sub>2</sub> confinement.

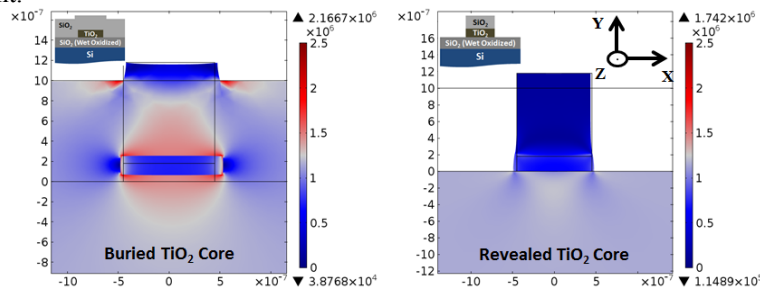


Fig. 4. Thermally induced stress profiles for Buried and revealed type waveguides. Figures are von Mises Stress profiles in Pa with a 10K temperature difference. A 10x displacement enhancement is applied for better visualization.

## 5. Conclusions

We have shown that TSO effects are important to performance of TiO<sub>2</sub> core waveguides most strongly indicated by reduction of the TOC by more than two orders of magnitude. Furthermore, we clarified the theoretical framework for this phenomenon with derivations of three models of ring resonator thermal drift. We believe that such buried channel waveguides show reduction in the thermal expansion of TiO<sub>2</sub> which is the likely cause of a stress induced suppression of the negative TOC in TiO<sub>2</sub>. Revealing the sidewalls to air appears to release that suppression. However, because of the complex nature of stress, each waveguide type requires numerical analysis to understand the role stress will play. Our model shows that in many cases this effect is at least as significant as non-stress related thermo-optic effects of the material and thus must be included to determine the correct TOC of TiO<sub>2</sub>. To generally solve the thermal drift problem without polymers or active feedback further stress research into TiO<sub>2</sub> is required to enable CMOS compatible athermal photonic integrated circuits.

## Acknowledgments

The authors acknowledge Sudharsanan Srinivasan and Martijn Heck for helpful discussions on theoretical details of this paper and support from Intel ARO program, and Semiconductor Research Corporation (SRC) for funding this research.